Int. J. Therm. Sci. (2000) 39, 213–224

S1290-0729(00)00240-4/FLA

Numerical study of turbulent flow and heat transfer from an array of thick plates

Mahmood Yaghoubi *, Mohamad Rahnema

Mechanical Engineering Department, Engineering School, Shiraz University, Shiraz, Iran

(Received 29 October 1998, accepted 16 July 1999)

Abstract — Convective heat transfer in turbulent flow from an array of blunt plates is numerically studied. The flow is assumed to be steady, two dimensional, incompressible and turbulent. A modified two equation k–ε model with the preferential dissipation modification is incorporated to determine accurately turbulent flow field, as well as the recirculation pattern along the entrance region of the plates. To predict the local variations of turbulence quantities in the k equation, a three-layer, near wall turbulence model was examined based on the wall function. The governing equations are solved using finite volume technique based on the bounded skew hybrid difference scheme BSHD, and the PISO algorithm to iterate for pressure corrections. The solutions were obtained using a two-pass procedure, devised to allow for the correct use of the wall functions. Computations for Re_D were obtained in the range $2.5{\cdot}10^4$ to 10^6; Prandtl numbers of 1, 2, 5, and 10 and blockage ratios of 5 % through 30 %. Results of friction coefficient, and Nusselt number distribution for the combined entry length problem are presented for different flow conditions and plates thickness. These findings are in accord with previously published experimental and theoretical results of a single plate. © 2000 Éditions scientifiques et médicales Elsevier SAS

forced convection / turbulent flow / parallel thick plates

Nomenclature

Br	blockage ratio, D/H	
C_μ, C_1, C_2	constant coefficients	
C_1', C_1''	coefficients in the modified k–ε turbulence model	
C_f	friction factor, $\mu(\partial u/\partial x)_x/(\rho u_\infty^2)$	
C_p	pressure coefficient, $(p-p_\infty)/(\rho u_\infty^2)$	
D	plate thickness	m
E	integration constant in logarithmic law of the wall (9.0)	
f_μ, f_ε	damping function in the k and ε equations	
G	generation term in k equation, equation (7)	
H	distance between centerlines of the plates	m
k	turbulent kinetic energy	$m^2{\cdot}s^{-2}$
k_{in}	turbulent kinetic energy at the inlet	$m^2{\cdot}s^{-2}$
k_p	turbulent kinetic energy of the first grid point near the wall	$m^2{\cdot}s^{-2}$
p	static fluid pressure	Pa
p_∞	upstream fluid static pressure	Pa
Pr	Prandtl number, ν/α	
Pr_t	turbulent Prandtl number, ν_t/α_t	
Re_D	Reynolds number, $u_\infty D/\nu$	
Re_{Dh}	Reynolds number based on hydraulic diameter, $2Hu_\infty/\nu$	
T	temperature	K
T_w	wall temperature	K
T_∞	upstream fluid temperature	K
T_p	fluid temperature of the first grid point near the wall	K
u_1, u_2	velocity components in x_1 and x_2 direction	$m{\cdot}s^{-1}$
U_p	velocity component in x_1 direction of the first grid point near the wall . .	$m{\cdot}s^{-1}$
u_∞	upstream fluid velocity	$m{\cdot}s^{-1}$
x_1, x_2	streamwise and cross-stream coordinates	m
x_r	reattachment length	m
y_p^+	wall coordinate $C_\mu^{1/4}k^{1/2}y/\nu$ at node p adjacent to the wall	

* Correspondence and reprints.
yaghoub@succ.shirazu.ac.ir

Greek symbols

α	thermal diffusivity	$m^2 \cdot s^{-1}$
α_t	turbulent thermal diffusivity	$m^2 \cdot s^{-1}$
κ	von Karman constant	
τ	shear stress	Pa
τ_w	wall shear stress	Pa
ε	dissipation rate of turbulent kinetic energy	$m^2 \cdot s^{-3}$
μ	dynamic viscosity	Pa·s
θ	dimensionless temperature, $(T - T_\infty)/(T_w - T_\infty)$	
$\sigma_k, \sigma_\varepsilon$	turbulent Prandtl number for diffusion of k and ε	
ν	kinematic viscosity of fluid	$m^2 \cdot s^{-1}$
ν_t	turbulent viscosity	$m^2 \cdot s^{-1}$
ν_{eff}	effective viscosity	$m^2 \cdot s^{-1}$
ρ	density	$kg \cdot m^{-3}$
ε_{in}	dissipation rate for turbulent kinetic energy at the inlet	$m^2 \cdot s^{-3}$

1. INTRODUCTION

Turbulent forced convection in the inlet section of parallel plates is commonly encountered in a variety of thermal engineering systems. For some applications, the plates are relatively thick and the flow is not of a boundary layer type accompanied by fluid separation and reattachment. These plates are met in heat exchangers, ducts and electronic devices to name a few. An understanding of the combined entry length problem for turbulent flow in such a row of parallel plates is important for thermal design processes. The nature of flow for such two-dimensional, thick, rectangular plates is sketched in *figure 1*. As the flow moves from left to right, the decrease in its velocity causes a favorable pressure gradient. The addition of pressure in the streamwise direction causes the flow to separate from the leading edge, and after a distance, to reattach to the plate, forming a recirculation bubble within which there is an adverse pressure gradient. Subsequently, the boundary layer begins and approaches the developed state. The mixing region between separation point and reattachment point plays an important role in heat and mass transfer processes. What follows is a brief review of the previous pertinent work in this area.

Theoretical and experimental analysis of fluid flow and heat transfer from horizontal parallel plates, and rectangular thin ducts have been studied in detail and a thorough review of these can be found in Shaw and Bathi [1]. For a single, thick plate with semi-infinite length, the analysis is also extensive. The contribution of Ota and his co-workers to understanding fluid flow and heat transfer for the single plate compose the fundamental studies. In their first article, Ota and Kon [2] explained an experimental investigation on heat transfer to determine the characteristic of turbulent flow of air over a blunt flat plate for $17\,900 > Re_D > 2\,720$. They studied a zero angle of attack plate and developed an empirical formula for the Nusselt number at the reattachment point. Under these conditions, they concluded that the flow reattachment occurred at about four-plate thickness from the leading edge. The position of the maximum Nusselt number is almost completely independent of the Reynolds number and zero shear stress was found to coincide with the reattachment point. Later Ota and Itasaka [3] studied such flow characteristics in more de-

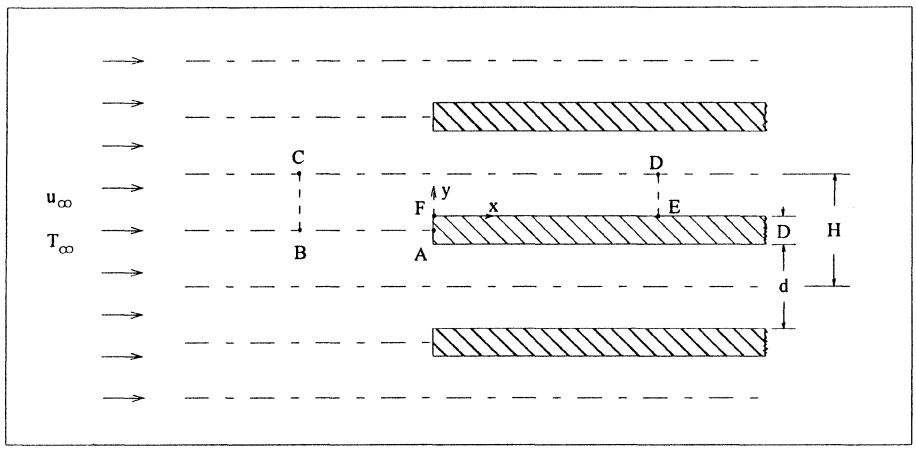

Figure 1. Geometry considered for an array of blunt plates.

tail for $66\,600 > Re_D > 21\,000$. It was shown that the boundary layer in the redeveloped flow region downstream of the reattachment is very thick, of approximately twice the plate thickness. Hillier and Cherry [4] also observed the Reynolds-number independent flow regime. They noted that the flow is essentially Reynolds number independent within the range: $34\,000 < Re_D < 80\,000$. In this study, it is shown that the flow is very sensitive to the grid generated and the free stream turbulence. Ota and Kon [5] have also studied the turbulent transfer of heat and momentum in separated and reattached flow over bluff bodies for $Re_D = 12\,000$. It was founded that the characteristic behavior of the turbulent heat flux appears to be similar to that of the turbulent shear stress in the separated and reattached flow region. In such conditions, the turbulent Prandtl number is general nearly equal to unity near the wall, and then it increases with the wall distance.

The experimental studies of Ota and Kato [6] and the recent measurements of Ota and Ohi [7] of turbulent heat transfer over a blunt plate for $Re_D = 5\,800$ show that the Nusselt number reaches a maximum at about 4.3 plate thickness while the reattachment point was located at 4.1 plate thickness. Also, it was mentioned that the vortex shedding from the reattachment region exhibits greater influences on the temperature field than the flapping motion of the separated shear layer. Furthermore, Coney et al. [8, 9] and Kazeminejad [10] published a series of papers of experimental studies on flow separation and reattachment.

Related numerical studies have also been made for a two-dimensional incompressible recirculating flow over bluff bodies. Benodekar et al. [11] studied turbulent flows over surface mounted ribs using a new computational method known as the bounded skew hybrid differencing scheme (BSHD) for incompressible recirculating flows. They compared their numerical results with the experimental findings and satisfactory improvements were observed over the previous results. More recently, Djilali, and his co-workers [12–14] performed a series of both numerical and experimental studies of turbulent flow over a bluff rectangular plate. In the experimental part, Djilali et al. [13] showed that the reattachment length and pressure distribution remained unchanged over the Reynolds number range $2.5{\cdot}10^4$ to $9.0{\cdot}10^4$. In the numerical computations, Djilali et al. [14] used a modified standard k–ε turbulence model and a variant that incorporates the curvature correction. Their results show that prediction of reattachment is very sensitive to the scheme of finite differencing and to turbulence modeling. They used two different discretization methods: hybrid differencing (HD) and bounded skew hybrid differencing (BSHD) schemes. It is found that BSHD, which has a higher differencing order, has better agreement for a reattachment length of 4.3 plate thickness with an experimental measurement of $4.7D$. The application of this scheme to turbulent recirculating flows has improved turbulent flow predictions [14, 15].

The influence of turbulence modeling is very important on heat, mass and momentum characteristics of the wall. Although the predictions of the flow away from the wall are generally not very sensitive to the near-wall turbulence model used, local heat transfer predictions are critically dependent on the near-wall model and considerable attention must be paid in the evaluation of the wall-proximity. For recirculating turbulent flows, Djilali et al. [12] has examined various near-wall turbulence models about two-dimensional blunt rectangular plates. They have found that the three-layer model of Amano [16] takes into account the variations of the turbulent kinetic energy k to evaluate the generation and destruction of k near the wall, and also predicts the Nusselt number along the plate with better agreements with the available experimental data. Recognizing this fact, the three-layer model is employed in the present numerical study.

Despite the contributions of the forgoing studies for the single plate much remains to be learned concerning the flow separation, reattachment, and development as well as heat transfer through an array of parallel blunt plates. As far as the authors are aware, detailed theoretical work on combined fluid flow and heat transfer for an array is very limited. The only related studies are for laminar flow for a stack of blunt plates by Djilali [17], and Rahnema et al. [18].

In the present study, the fluid flow characteristic and heat transfer rate from an array of parallel blunt plates with forced flow parallel to the plate surfaces, such as illustrated in *figure 1*, have been studied numerically. In this geometry an additional parameter plays an important role, known as blockage ratio (D/d). This work expands the turbulent heat transfer data on the combined entry length problem for parallel plate ducts, by considering the effects of plate thickness, plate spacing, flow Reynolds number and other various flow conditions. In order to check the accuracy of the numerical technique, the computed velocity profiles for fully developed turbulent flow in thin ducts as well as flow reattachment length for single plate are found and compared with those available in texts and subsequent agreement is observed.

Also shown for comparison are the variations of local friction coefficient with the distance along the plate for the forced convection turbulent boundary layer in thin ducts where significant differences were found in the entrance region.

2. MATHEMATICAL FORMULATION

The geometry and coordinate for the flow under consideration is illustrated in *figure 1*. It is assumed that flow is uniform and parallel with the plates. Thermophysical properties of the fluid are assumed to remain constant and the plates are thick such that the flow exhibits separation and reattachment. With these simplified assumptions, the computational domain can be isolated section ABCDEFA, as shown in *figure 1*. The governing equations for a two-dimensional, steady, turbulent flow of a Newtonian fluid are as follows.

- Continuity:

$$\frac{\partial u_j}{\partial x_j} = 0 \tag{1}$$

- Momentum:

$$u_j \frac{\partial u_i}{\partial x_j} = -\frac{1}{\rho}\frac{\partial p}{\partial x_i} + \frac{\partial}{\partial x_j}\left(\nu_{\text{eff}}\left(\frac{\partial u_i}{\partial x_j} + \frac{\partial u_j}{\partial x_i}\right)\right) \tag{2}$$

where

$$\nu_{\text{eff}} = \nu + \nu_{\text{t}} \tag{3}$$

The values of ν and ν_{t} are laminar and turbulent kinematic viscosity, respectively.

- Energy:

$$u_j \frac{\partial \theta}{\partial x_j} = \frac{\partial}{\partial x_j}\left[\left(\frac{\nu}{Pr} + \frac{\nu_{\text{t}}}{Pr_{\text{t}}}\right)\frac{\partial \theta}{\partial x_j}\right]$$

2.1. Turbulence modeling

Turbulence closure is implemented by a two-equation model and utilizes the kinetic energy k with a dissipation rate ε which enables the determination of the isotropic eddy viscosity according to

$$\nu_{\text{t}} = \frac{C_\mu k^2}{\varepsilon} \tag{4}$$

The equations for k and ε can be written as

$$u_j \frac{\partial k}{\partial x_j} = \frac{\partial}{\partial x_j}\left(\frac{\nu_{\text{eff}}}{\sigma_k}\frac{\partial k}{\partial x_j}\right) + G - \varepsilon \tag{5}$$

$$u_j \frac{\partial \varepsilon}{\partial x_j} = \frac{\partial}{\partial x_j}\left(\frac{\nu_{\text{eff}}}{\sigma_\varepsilon}\frac{\partial \varepsilon}{\partial x_j}\right) + C_1 \frac{\varepsilon}{k} G - C_2 \frac{\varepsilon^2}{k} \tag{6}$$

where G represents the generation of turbulent kinetic energy and is given by

$$G = \nu_{\text{t}} \frac{\partial u_i}{\partial x_j}\left(\frac{\partial u_i}{\partial x_j} + \frac{\partial u_j}{\partial x_i}\right) \tag{7}$$

The model constants are $C_\mu = 0.09$, $C_1 = 1.44$, $C_2 = 1.92$, $\sigma_k = 1.0$, and $\sigma_\varepsilon = 1.217$.

2.2. Turbulence model correction

In the standard k–ε turbulence model, it is assumed that the Reynolds stresses are isotropic tensor. With this assumption, the relation between Reynolds stress and mean velocity gradients can be expressed in the Stokes law. However, some authors have reported series of deficiencies in the k–ε turbulence model for some particular flows. For flows with strong streamline curvature, Leschziner and Rodi [15] found that the measured anisotropy of the normal stresses and the magnitude of the shear stresses are not well predicted by k–ε model. Extensive attempts have been made to modify the k–ε model and improve its performance for complex flows. In the present analysis the modification suggested by Leschziner and Rodi [15] for recirculating flows is accepted. Such modification already demonstrated better flows of the same type [14]. By this scheme, the term representing "production of dissipation" in the ε equation, $P_\varepsilon = C_1(\varepsilon/k)G$, is replaced by

$$P'_\varepsilon = \frac{\varepsilon}{k}\left(C'_1 G - C''_1 \nu_{\text{t}} S^2_{\text{ns}}\right) \tag{8}$$

where $C'_1 = 2.24$ and $C''_1 = 0.8$ (giving, consistently with the standard k–ε model, $C'_1 - C''_1 = C_1$). The shear strain in the direction of the streamline, S_{ns}, is calculated similar to Leschziner and Rodi [15].

2.3. Boundary conditions

The solution of the above elliptic equations requires that the boundary conditions be specified along the entire boundaries that enclose the flow field. For locations close to the solid boundaries the most common form of the wall functions, first proposed by Launder and Spalding [19], imply the existence of a near-wall linear sublayer, where the momentum transfer is dominated by molecular viscosity and heat transfer by conductivity, followed by a logarithmic region. In this model, a parabolic variation of turbulent kinetic energy is assumed, which corresponds to the linear increase of fluctuating velocity with distance from the wall within the viscous sublayer. The turbulent kinetic energy k is zero on the wall and varies linearly toward the outer node points. The turbulent shear stress is zero within the viscous sublayer and the shear stress undergoes an abrupt increase at the edge of the

sublayer while varying linearly over the remainder of the cell. For boundary conditions related to the momentum equations and the two equations of k and ε, a two-layer model is employed but to satisfy the energy equation a near-wall three-layer model is employed. According to the above assumptions, the boundary conditions for the region ABCDEFA shown in *figure 1* are as follows.

On the rigid walls, the standard wall boundary conditions are used and for other quantities, the following conditions exist:

- Wall shear stress:

$$\tau_w = \rho\kappa C_\mu^{1/4} k_p^{1/2} \frac{U_p}{\ln(E y_p^+)} \quad \text{if } y_p^+ \geq 11.63 \tag{9}$$

$$\tau_w = \mu \frac{U_p}{y_p} \quad \text{if } y_p^+ \leq 11.63 \tag{10}$$

where U_p and y_p are the streamwise velocity components and the distance from the wall for the nearest grid point adjacent to the wall and E and κ are integration constant in the logarithmic law of the wall and von Karman constant. This expression is used to evaluate the near wall diffusion terms in the momentum equations.

- Turbulent kinetic energy:

$$\varepsilon = \frac{C_\mu^{3/4} k^{3/2}}{\kappa y_p} \ln\left(E y_p^+\right) \tag{11}$$

The dissipation rate from this expression is used to evaluate the dissipation term $-\varepsilon$ in the k equation.

- Dissipation rate: for the node adjacent to the wall, equation (6) is not used, and the value of ε is evaluated under local equilibrium conditions as

$$\varepsilon = C_\mu^{3/4} \frac{k_p^{3/2}}{\kappa y_p} \tag{12}$$

- Temperature: for a constant wall heat flux q_w'', the wall temperature is obtained from

$$T^+ = \frac{(T_w - T_p)\rho C_p C_\mu^{1/4} k_p^{1/2}}{q_w''} = Pr_t \left[\frac{1}{k}\ln\left(E y^+\right) + P\right]$$

where the empirical P function of Jayetilleke [20] is given by

$$P = 9.24\left[\left(\frac{Pr}{Pr_t}\right)^{3/4} - 1\right]\left[1 + 0.28\exp\left(-0.007\frac{Pr}{Pr_t}\right)\right]$$

For section BC at the inlet the following values are assumed:

$$u_1 = u_\infty, \quad u_2 = 0.0, \quad k_{in} = 6.4 \cdot 10^{-5} u_\infty^2$$
$$\varepsilon_{in} = \frac{k_{in}^{1.5}}{1.1 \cdot 10^{-2} H} \tag{13}$$

where H is the distance between centerlines of thick plates.

For section DE at the outlet, the zero-gradient boundary condition is used:

$$\frac{\partial(\Theta)}{\partial x} = 0.0 \quad \text{for } \Theta \text{ equal to } u_1, u_2, k, \varepsilon, \text{ and } \theta \tag{14}$$

This condition is used for computational convenience. Although it is not strictly valid when the flow is not fully developed at the outlet boundary, its use is permissible when this boundary is located (1) in a region where the flow is in the downstream direction, and (2) sufficiently far downstream from the region of interest. For sections BA and CD, the symmetric boundary condition is used.

2.4. Three-layer near-wall model

Due to the deviation of the linear and logarithmic profile from experimental data in the buffer layer, $5 < y^+ < 30$, it seems that the three-layer near-wall model may result in a better prediction than the two-layer model and other near wall models in estimating friction factor and heat transfer from the wall. The three-layer model is composed of a viscous sublayer $0 < y^+ < 5$, adjacent to the wall, a buffer layer, $5 < y^+ < 30$, and an overlap layer $30 < y^+ < 400$, such as illustrated in *figure 2*.

Figure 2 shows a computational node p whose associated control volume is bounded by a wall on the south side. Amano [16] originally proposed two-layer and three layer near-wall models as explained and numerically compared with other near wall turbulence models by Djilali et al. [12]. Here, only the three-layer model is explained, but more detail can be found in Amano [16] and Djilali et al. [12].

The three layers are shown such that the node point P lies outside the buffer layer, assuming the near-wall cell is large enough. The behavior of the turbulence kinetic energy k, ε and the turbulence shear stress τ can be summarized in the following form of the three layers:

- Viscous sublayer ($0 < y^+ < 5$):

$$k = k_v \left(\frac{y}{y_v}\right)^2$$
$$\varepsilon = 2\nu\left(\frac{\partial k^{1/2}}{\partial y}\right)^2 \tag{15}$$
$$\tau = 0$$

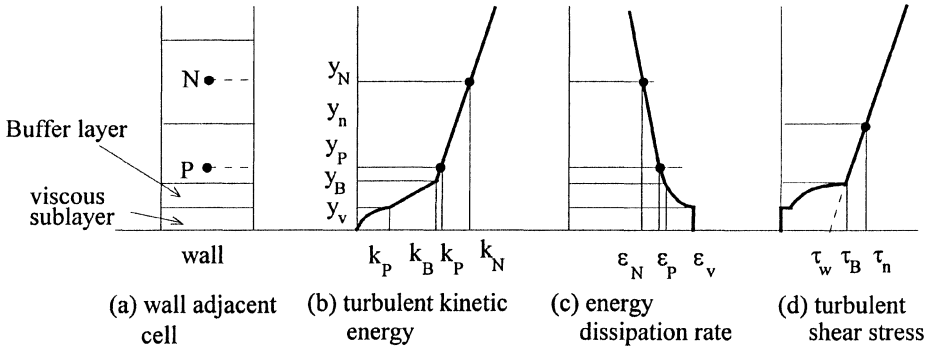

Figure 2. Near-wall three-layer model.

- Buffer sublayer ($5 < y^+ < 30$):

$$k = k_B \frac{y}{y_B}$$
$$\varepsilon = \frac{k^{3/2}}{c_l y} \tag{16}$$
$$\tau = \tau_B \left(\frac{y}{y_B}\right)^3$$

- Fully turbulent region ($30 < y^+ < 400$):

$$k = \frac{k_n - k_B}{y_n - y_B} y + \left(k_p - \frac{k_p - k_N}{y_p - y_N} y_p\right) = by + a$$
$$\varepsilon = \frac{k^{3/2}}{cy} \tag{17}$$
$$\tau = \tau_w + (\tau_n - \tau_w)\frac{y}{y_n}$$

where

$$a = k_p - \frac{k_p - k_N}{y_p - y_N} y_p$$
$$b = \frac{k_n - k_B}{y_n - y_B}$$

Details of the formulation for the variation of k, ε and τ are given by Amano [16]. The mean generation and destruction rates for k equation will be obtained as follows:

$$\overline{G} = \frac{\tau_w(U_n - U_B)}{y_n} + \frac{\tau_B}{4y_B^3 y_n}\left(y_B^4 - y_v^4\right)\left(\frac{\partial U}{\partial y}\right)_{BZ} + \frac{\tau_w(\tau_n - \tau_w)}{\rho\kappa^* k_B^{1/2} y_n}\left(1 - \frac{y_B}{y_n}\right) + \left\{\tau_w\left(1 - \frac{y_B}{y_n}\right) + \frac{\tau_n - \tau_w}{2}\left[1 - \left(\frac{y_B}{y_n}\right)^2\right]\right\} \cdot \left(\frac{\partial V}{\partial x}\right)_{FTR} \tag{18}$$

Here the subscripts BZ and FTR stand for buffer zone and fully turbulent region, and $(\partial V/\partial x)_{BZ}$ is assumed to be negligible. The mean dissipation rate for the k equation is obtained by following relation:

$$\bar{\varepsilon} = \frac{2k_v^{3/2}}{y_n R_v} + \frac{1}{y_n C_l}\left\{\frac{2}{3}k_B^{3/2}\left[1 - \left(\frac{y_v}{y_B}\right)^{3/2}\right] + \frac{2}{3}\left(k_n^{3/2} - k_B^{3/2}\right) + 2a\left(k_n^{1/2} - k_B^{1/2}\right) + a^2\lambda\right\} \tag{19}$$

where

$$\lambda = \begin{cases} \dfrac{1}{a^{1/2}} \ln\left[\dfrac{(k_n^{1/2} - a^{1/2})(k_B^{1/2} + a^{1/2})}{(k_B^{1/2} - a^{1/2})(k_n^{1/2} + a^{1/2})}\right] \\ \quad \text{if } a > 0 \\ \dfrac{2}{(-a)^{1/2}}\left[\tan^{-1}\left(\dfrac{k_n}{-a}\right)^{1/2} - \tan^{-1}\left(\dfrac{k_B}{-a}\right)^{1/2}\right] \\ \quad \text{if } a < 0 \end{cases}$$

The mean generation and destruction rate of the ε equation can be determined in the same manner. Use of these near-wall models for determining heat transfer characteristics for a backward step has improved significantly with results obtained by experimental data. This model was also used for flow around a blunt plate by Djilali et al. [12], which showed improvement in the prediction of Nusselt number along the plate surface compared with the standard wall function method. The evaluation of the dependent variables close to the wall has proven satisfactory, hence it is used in the present investigation.

3. NUMERICAL SCHEME

The governing equations (1)–(6) are discretised by a finite volume procedure. Velocity components were

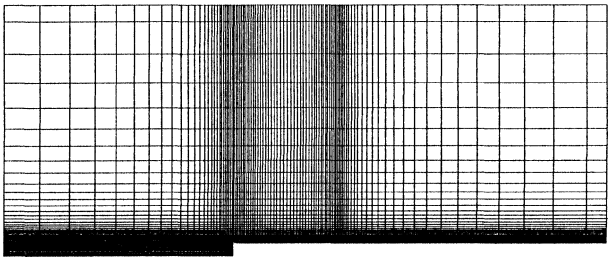

Figure 3. Grid distribution for turbulent computation.

stored at the staggered locations, while the pressure and temperature were considered at the main grid points. The Bounded Skew Hybrid Differencing Scheme (BSHDS) is employed for discretizing convective terms in the momentum equations. By considering the local direction of the flow, the BSHD scheme involves differencing the equations in terms of the variables at nodes on north, south, east, and west sides of the grid point, and to a lesser extent, in terms of the values on the nodes labeled NE, NW, SE, and SW. By considering the local direction of the flow, the BSHD scheme greatly reduces false numerical diffusion that results from the non-alignment of the coordinate grid with the flow direction, Raithby [21], and Lai, and Gosman [22]. A staggered non-uniform grid is used for the present computations, as illustrated in *figure 3*. The solution is obtained by an iterative method along with the pressure correction algorithm PISO (Pressure Implicit Split Operation) of Issa [23]. A modified TEACH-II code by Benodaker et al. [24] incorporates the BSHD/PISO, and is used in the present calculations. In this study, the set of difference equations is solved iteratively, line-by-line, in conjunction with the Thomas algorithm. Computation was started by first solving the continuity, momentum and k–ε equations to determine the flow field, and then by solving the energy equation to find the thermal field in the region of interest.

The computational region extends $10D$ upstream and $15D$ downstream from the leading edge in the x_1 direction and half the plate spacing in the transverse direction. Expansion of the computational domain revealed no significant changes in the flow field. The numbers of grid points in the x_1 and x_2 directions were 100×72, respectively. Fine grid spacing is used in the recirculating region along with a variable grid size on the rest of the domain. Variable grid spacing is used to resolve steep gradients of velocity near the wall in a transverse direction, as illustrated in *figure 3*. To achieve high accuracy of the flow field, the minimum value of Δx_1 and Δx_2 is taken as 0.06 and 0.01 of the plate thickness, respectively. The grid expansion factor in the x_1 and x_2 direction is taken as less

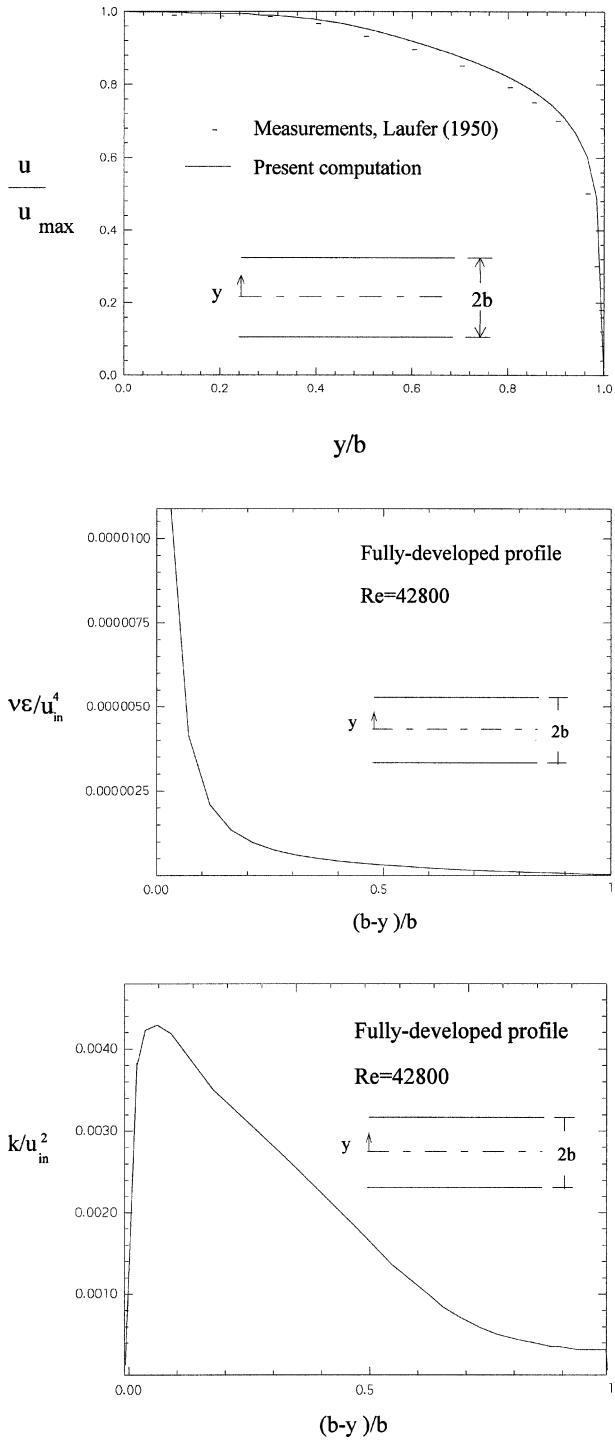

Figure 4. (a) Fully developed turbulent velocity profile between parallel plates. (b) Profile of dissipation of turbulent kinetic energy in a smooth flat duct at $Re = 42\,800$, computed with modified k–ε turbulence model. (c) Distribution of kinetic energy in a smooth flat duct at $Re = 42\,800$ computed with modified k–ε turbulence model.

than 1.2. The use of coarse grids resulted in a shorter recirculation length.

For study of the flow field, the numerical scheme began with an initial condition of uniform values for all variables. For some cases, an attempt was made to accelerate convergence by applying different initial conditions. For instance, solving at a higher Reynolds number, the solution obtained from a lower Reynolds number was used as an initial condition. Convergence of the computations is declared when the maximum value of residuals for mass, momentum and energy is less than $2{\cdot}10^{-3}$.

For validation purposes, comparison is made of the present computational method with the solution of the Coutte flow in a two-dimensional channel. *Figure 4a* shows the comparison of the predicted velocity profile with the experimental measurements of Laufer [25] for a fully developed turbulent condition.

Figures 4b and *4c* illustrate predicted turbulent kinetic energy and the distribution of turbulent kinetic energy dissipation rate corresponding to *figure 4a*. The values of k and ε in these figures are nondimensionalized with respect to the fluid inlet conditions. The value of k is zero over the wall and then it increases sharply away from the wall. However, the gradient of both k and ε drops to zero at the centerline of the duct.

It is evident that our numerical predictions for velocity profile are in conjunction with the measurements in ducts with thin walls. This comparison along with further studies in the next section reveal that the present model can accurately simulate the flow field and heat transfer between parallel plates.

4. RESULTS AND DISCUSSIONS

4.1. Fluid flow

The flow for the present problem, *figure 1*, can be divided into three regions: the upstream section before the plate, the section between separation and reattachment, and the downstream part where the boundary layer grows freely along the duct until it is fully developed to about one half of the plate spacing. There is slight pressure reduction at the leading edge due to flow acceleration and adverse pressure gradients in the recirculating zone. Pressure reduction continues as the fluid flows through the duct. The reattachment point is determined by the linear interpolation of the computed wall's shear stress distribution along the plates. The typical velocity vector field in the entrance region of the duct for

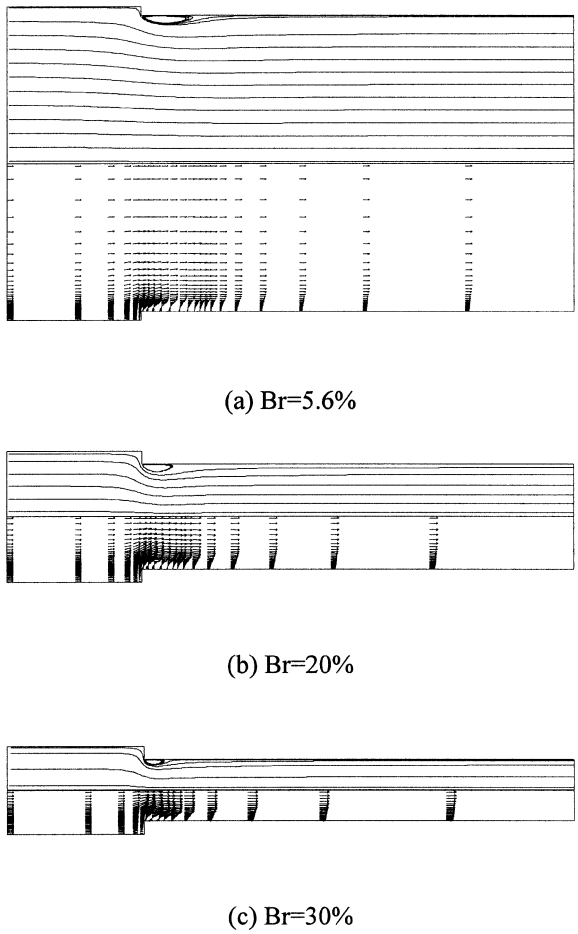

Figure 5. Typical velocity field for various blockage ratios.

blockage ratios of 5.6 %, 20 % and 30 % and for Re_D, illustrated in *figure 5*. In this figure the plate thickness is assumed to be constant, while the plate spacing is decreased. The flow reversal in the recirculating region, as well as boundary layer development, is clearly visible over the plate. The reattachment length is a function of both the Reynolds number and blockage ratio. For $Br = 5.6\,\%$ and $Re_D = 50\,000$, the value of x_r/D is about 4.35. This statement agrees well with those reported by the experimental observation of 4.7 made by Djilali and Gratshore [13] and also with the numerical predictions of 4.3 made by Djilali et al. [14]. Comparison of the present study with data of the other analysis verifies the accuracy of the present computation procedure. The variation of recirculation length and its inverse proportionality with Br is presented in *figure 6*. The following relation can correlate numerical calculations:

$$\frac{x_r}{D} = -0.1125Br + 4.875 \qquad (20)$$

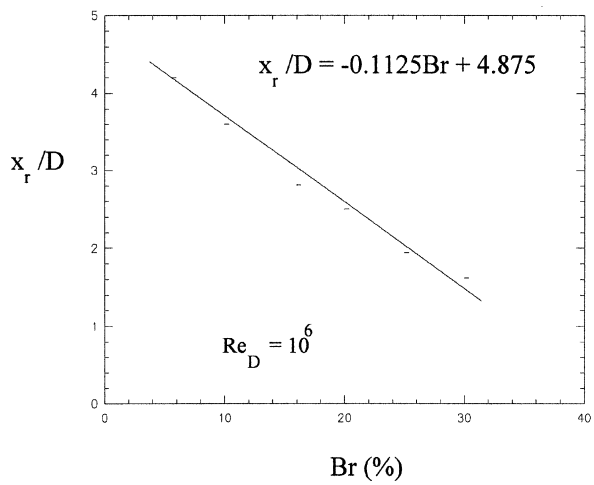

Figure 6. Variation of reattachment length with blockage ratio.

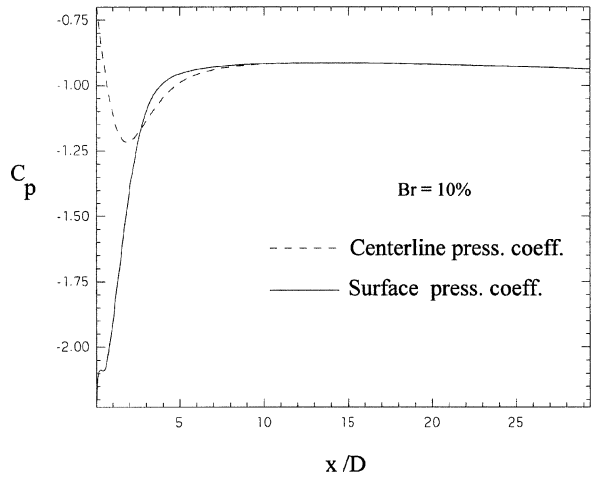

Figure 7. Comparison of surface pressure coefficient with that of centerline for $Br = 10\,\%$ and $Re_{\mathrm{D}} = 50\,000$.

Figure 7 illustrates variation of the centerline and plate surface pressure coefficient along the duct. Pressure in the entrance section where recirculation occurs is different but they both approach the same value after reattachment, thereafter it decreases along the duct that eventually should approach the fully developed condition. However, the pressure reduction close to the tip is more pronounce than it is at the duct centerline.

4.2. Friction

The variation of friction coefficient

$$C_{\mathrm{f}} = \frac{(\mu \partial u/\partial y)_{y=0}}{\frac{1}{2}\rho u_{\infty}^2}$$

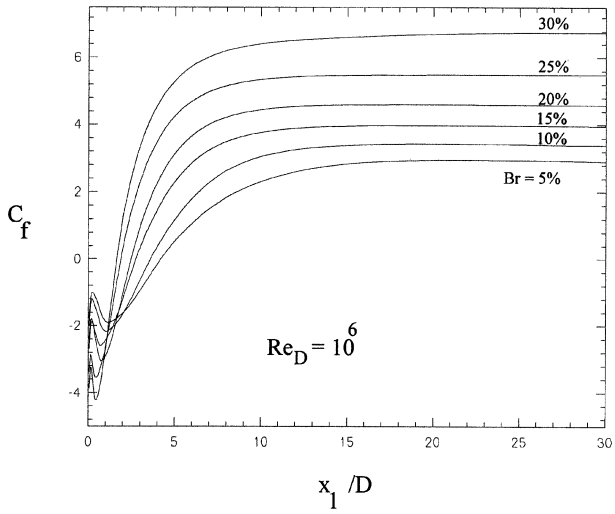

Figure 8. Variation of friction coefficient with blockage ratio along the duct.

in the entrance region of the plates for $Re_{\mathrm{D}} = 50\,000$ and different values of Br are illustrated in *figure 8*. In this graph each blockage ratio belongs to a certain Re. Note that $Re = 2Re_{\mathrm{D}}(1 + 1/Br)$. It can be seen that the blockage ratio has strong effects on the value C_{f}. The friction coefficient has a negative value in the beginning, due to the reverse flow close to the wall and zero value at the reattachment point. After the reattachment, C_{f} increases to a high value. The higher the blockage ratio the larger the friction coefficient after the reattachment point. This effect is due to the reduction of both the separation bubble length and the short distance that the flow has to develop after the bubble. The value of C_{f}, however, decreases as the flow moves toward the fully developed condition for all blockage ratios. By reducing the blockage ratio, the value of C_{f} approaches that of thin duct.

4.3. Heat transfer

For flow through parallel plates with finite thickness, D, the fluid flow and heat transfer depends on the Reynolds number Re_{D}, Prandtl number Pr, and blockage ratio, $Br = D/d$. For the combined entry length problem, it is common to plot the results against the distance along the duct.

For further evaluation of the computational results, comparison is made by plotting the Nusselt number for $Re_{\mathrm{D}} = 25\,000$, using standard k–ε model (STD), three-layer k-zone model as well as the measurements of Ota and Kon [26] for a single semi-infinite plate

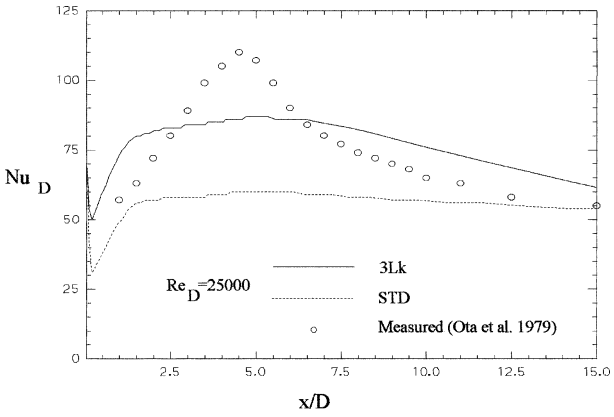

Figure 9. Comparison of experimental results with numerical computation of Nusselt number distribution along an isolated plate.

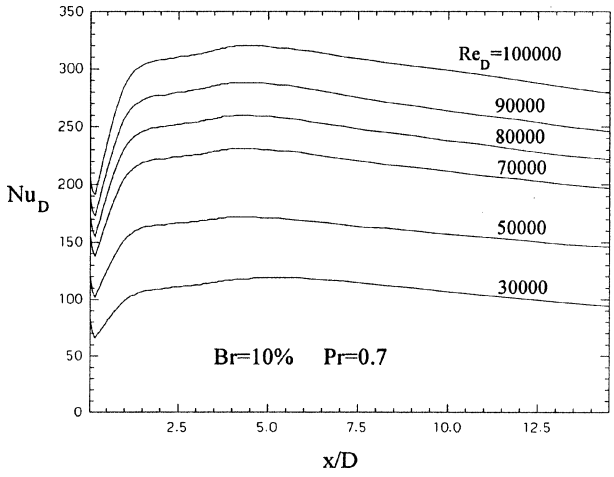

Figure 10. Variation of Nusselt number along the plate with Reynolds number for $Br = 10\,\%$ and $Pr = 0.70$.

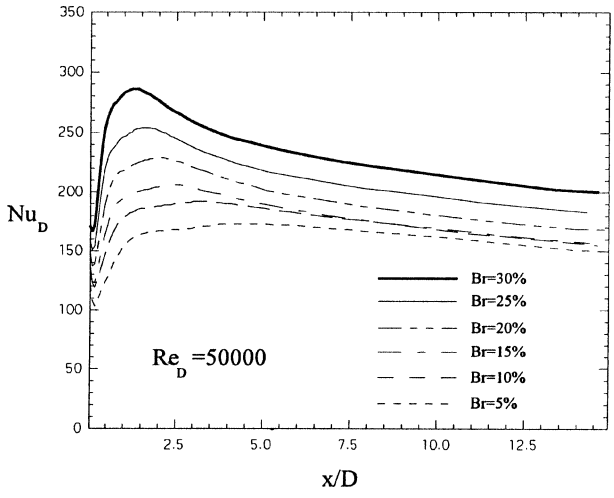

Figure 11. Variation of Nusselt number along the plate with blockage ratio for $Re_D = 50\,000$.

as shown in *figure 9*. For any particular Re_D, Nusselt number begins at a low level, except at $x = 0$, which is a singular point, then increases as it moves away from the leading edge; and then it decreases, eventually following the boundary layer development. As seen from this figure, the prediction of Nu_D from standard wall function (STD) is far from the experimental data, while that of the three-layer for k equation has shifted closer to the measurements in the recirculation region. The error in the maximum Nusselt number for the isolated plate is about 25 %. This difference may be due to differences in experimental conditions with numerical computation, regarding plate surface roughness, turbulent intensity of incoming stream and relative errors in measurements. Overall, based on poor performances of the standard wall function (STD), all computations for parallel plates are made using the three-layer k model. These results are quite acceptable, considering the complexity of the reattachment process.

Variation of Nu_D for $Br = 10\,\%$ and various Reynolds numbers are illustrated in *figure 10*. For each Re_D, there is a maximum of Nu_D, which corresponds to the reattachment position and the general variation of Nu_D along the duct and does not change significantly. It should be noted that the position of maximum Nu_D is the same for all Re_D. This is due to the fact that the reattachment length is nearly constant for $Re_D > 3{\cdot}10^4$. Heat transfer increases considerably with Reynolds number and after reattachment it decreases toward a fully developed condition. The variation of heat transfer coefficient along the plate for different blockage ratios and $Re_D = 5{\cdot}10^4$ is illustrated in *figure 11*. As displayed, it reveals that as the reattachment length gets smaller (plate thickness decreases) the location of the maximum Nusselt number approaches the leading edge and its relative value increases. Based on the above numerical computations, the variation of the maximum Nusselt number for different Reynolds number and blockage ratios for $Pr = 0.7$ is illustrated in *figure 12*. For such a specific ratio of Nu and Re_D a linear profile with blockage ratio is observed. *Figure 13* shows the variation of Nu_D for various Prandtl numbers, $Re_D = 10^6$ and $Br = 10\,\%$ along the duct entrance region. Nusselt number is large at first; then it drops due to flow reversal and increases again because of flow reattachment. After reattachment, Nusselt number asymptotically approaches the limiting value for long ducts further down stream. However, for all cases the limiting value of Nusselt number is the same as it should be

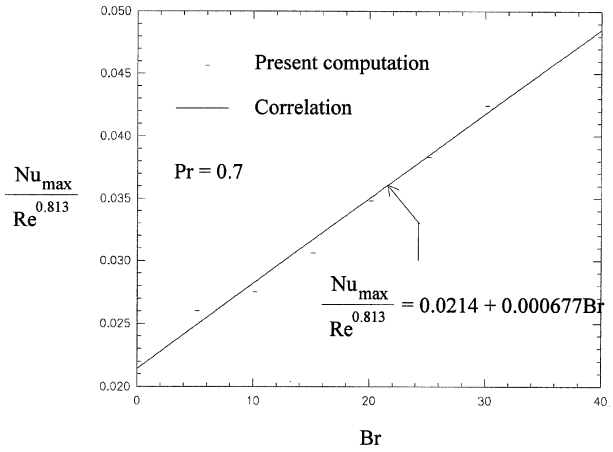

Figure 12. Variation of maximum Nusselt number with blockage ratio for $Pr = 0.7$.

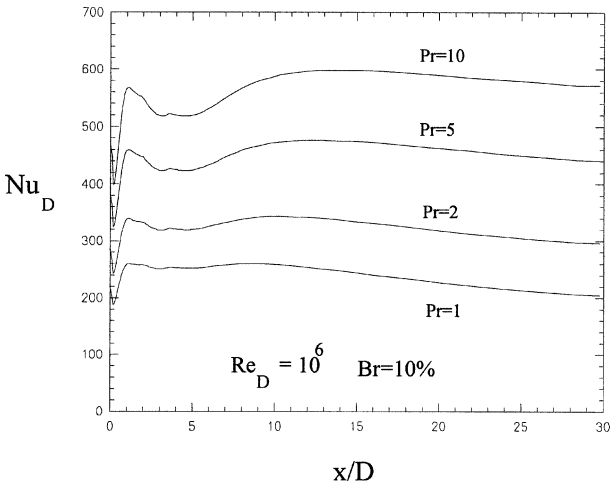

Figure 13. Variation of Nusselt number along the plate with Pr for $Re_D = 10^6$ and $Br = 10\%$.

attained at a constant value for the fully developed condition. This figure shows that Nusselt number and its variation in the entrance region exhibit pronounced effects with large Pr.

5. CONCLUSION

Turbulent fluid flow and heat transfer in the entrance region of a series of blunt plates accompanying with separation, reattachment and boundary layer development have been studied numerically. Based on this analysis the following conclusion can be made.

1. The result of BSHD computation scheme along with the use of preferential dissipation modification of the k–ε model as well as the three-layer k model for the wall function improved the prediction of convection heat transfer in the entrance region of the blunt plates and the results are sufficiently accurate for engineering purposes. However, more experimental investigations are required to establish more reliable calculation.

2. For the range of the present studies, reattachment length and flow field are independent of the Reynolds number, but depend on the blockage ratio by the following relation:

$$\frac{x_r}{D} = -0.1125Br + 4.875$$

$$30\,\% > Br > 5\,\%, \qquad 2.5{\cdot}10^4 < Re_D < 10^6$$

3. The friction coefficient, C_f, along the entrance section of the duct is different from those of thin ducts. The higher the blockage ratio, the larger the value of friction coefficient in the entrance zones. However, as the duct thickness decreases, C_f approaches thin ducts. For a high value of x/D, friction coefficient approaches a constant value, which resembles the fully developed condition in the duct.

4. For plate with uniform and constant heat flux, convective heat transfer depends on the flow blockage ratio and reveals a maximum near the reattachment point, while it decrease along the plate until it reaches the fully developed condition.

5. The entrance region effects are greater for higher Prandtl number fluid and lesser for low Prandtl number fluids.

Acknowledgement

This work is supported by Shiraz University Research Council.

REFERENCES

[1] Shah R.K., Bhatti M.S., Laminar convection heat transfer in ducts, in: Shah R.K., Kakac S., Aung N.A. (Eds.), Handbook of Single-Phase Convection Heat Transfer, Wiley, New York, 1987.

[2] Ota T., Kon N., Heat transfer in the separated and reattached flow on a blunt flat plate, Trans. ASME, J. Heat Transfer 96 (1974) 459–462.

[3] Ota T., Itasaka M., A separated and reattached flow on a blunt flat plate, ASME J. Fluid Engrg. 98 (1976) 79–87.

[4] Hiller R., Cherry N.J., The effect of stream turbulence on separation bubbles, J. Wind Engineering and Ind. Aero. 8 (1981) 49–58.

[5] Ota T., Kon N., Turbulent transfer of momentum and heat in a separated and reattached flow over flat plate, ASME J. Heat Transfer 102 (1980) 749–754.

[6] Ota T., Kato N., Turbulent heat transfer in a separated and reattached flow over a blunt flat plate, ASME/SSMAE Thermal Engineering Proceedings 3 (1991) 191–196.

[7] Ota T., Ohi N., Turbulent heat transfer in a separated and reattached flow over a blunt flat plate, in: ASME/JSME Thermal Engineering Conference 1 (1995) 363–370.

[8] Coney J.E.R., Kazeminejad H., Sheppard C.G.W., Experimental study of separated flow over a thick plate, in: 2nd UK National Conference on Heat Transfer, Glasgow, U.K. 1 (1988) 761–772.

[9] Coney J.E.R., Kazeminejad H., Sheppered C.G.W., Experimental study of forced convective heat transfer in separated flow, in: 2nd National Conference on Heat Transfer, Glasgow, U.K. 1 (1988) 701–716.

[10] Kazeminejad H., Measurement of local convective heat transfer coefficient using an electrically heated thin copper-coated plastic sheet, Iranian J. of Science and Technology 21 (1) (1997) 69–86.

[11] Benodekar R.W., Goddard A.J.H., Gosman A.D., Issa R.I., Numerical prediction of turbulent flow over surface mounted ribs, AIAA J. 23 (1985) 359–366.

[12] Djilali N., Gratshore I., Salcudean M., Calculation of convective heat transfer in recirculating turbulent flow using various near-wall turbulence models, Numerical Heat Transfer, Part A 16 (1989) 189–212.

[13] Djilali N., Gratshore I.S., Turbulent flow around a bluff rectangular plate, Part I: Experimental investigation, J. Fluid Engrg., ASME Trans. 113 (1991) 51–59.

[14] Djilali N., Gratshore I.S., Sacludean M., Turbulent flow around a bluff rectangular plate, Part II: Numerical predictions, J. Fluid Engrg., ASME Trans. 113 (1991) 60–67.

[15] Leschziner M.A., Rodi W., Calculation of annular and thin parallel jets using various discretization schemes and turbulence model variation, ASME J. Fluid Engrg. 103 (1981) 352–360.

[16] Amano R.S., Development of a turbulence near-wall model and its application to separated and reattached flows, Numerical Heat Transfer 7 (1984) 59–75.

[17] Djilali N., Forced laminar convection in an array of stacked plates, Numerical Heat Transfer, Part A 25 (1994) 393–408.

[18] Rahnema M., Yaghoubi M., Kazeminejad H., A numerical study of convective heat transfer from an array of parallel blunt plates, Internat. J. Heat Fluid Flow 18 (1997) 430–436.

[19] Launder B.E., Spalding D.B, The numerical computation of turbulent flows, Comp. Meth. Appl. Mech. Engrg. 3 (1974) 269–289.

[20] Jayatilleke C.L.V., The influence of Prandtl number and surface roughness on the resistance of laminar sublayer to momentum and heat transfer, Progress in Heat and Mass Transfer 1 (1969) 193–329.

[21] Raitby G.D., Skew upstream differencing for problem involving fluid flow, Comp. Meth. Appl. Mech. Engrg. 19 (1978) 153–164.

[22] Lai K.Y.M., Gosman A.D., Finite difference and other approximations for the transport and Navier–Stokes solutions, Dept. Mech. Engrg., Imperial College, London, U.K., Report FS/82/16, 1982.

[23] Issa R.I., Solution of implicitly discretized fluid equations by operator-splitting, Internal Report, Dept. of Mineral Resources Engineering, Imperial College, London, U.K., 1982.

[24] Benodekar R.W., Gosman A.D., Issa R.I., The TEACH code for the detailed analysis of two-dimensional turbulent recirculation flow, Dept. Mech. Engrg., Imperial College, London, U.K., Report FS/83/3,1983.

[25] Laufer J., Some recent measurements in a two-dimensional turbulent channel, J. Aerospace Science 17 (1950) 277–287.

[26] Ota T., Kon N., Heat transfer in the separated and reattached flow over flat plates-effects of noise shape, Int. J. Heat Mass Tran. 22 (1979) 197–206.